Title
Drag Forces Experienced By Two, Full-scale Vehicles At Close Spacing

Authors
Hong, Patrick
Marcu, Bogdan
Browand, Fred
et al.

Publication Date
1998

CALIFORNIA PATH PROGRAM
INSTITUTE OF TRANSPORTATION STUDIES
UNIVERSITY OF CALIFORNIA, BERKELEY

Drag Forces Experienced by Two, Full-Scale Vehicles at Close Spacing

Patrick Hong, Bogdan Marcu, Fred Browand, Aaron Tucker
University of Southern California

California PATH Research Report
UCB-ITS-PRR-98-5

This work was performed as part of the California PATH Program of the University of California, in cooperation with the State of California Business, Transportation, and Housing Agency, Department of Transportation; and the United States Department of Transportation, Federal Highway Administration.

Report for MOU 245

February 1998

ISSN 1055-1425

Drag Forces Experienced by Two, Full-Scale Vehicles at Close Spacing

Patrick Hong
Bogdan Marcu
Fred Browand
Aaron Tucker

Department of Aerospace Engineering
University of Southern California
Los Angeles, California 90089-1191
Fax (213)740-7774

This work is supported by the California Department of Transportation, under the auspices of the California PATH Program, UC Berkeley.
Draft No. D97-125.

Graduate Student	Research Associate	Professor	Graduate Student
Patrick Hong	Bogdan Marcu	Fred Browand	Aaron Tucker
phong@spock.usc.edu	marcu@spock.usc.edu	browand@spock.usc.edu	atucker@scf.usc.edu
(213) 740-5320	(213) 740-7183	(213) 740-5359	(213) 740-5320

EXECUTIVE SUMMARY

The present study aims to document the drag reduction for a two-vehicle platoon by operating two full-scale Ford Windstar vans in tandem on a desert lakebed. Drag forces are measured with the aid of a special tow bar force measuring system designed and manufactured at USC. The testing procedure consists of a smooth acceleration, followed by a smooth deceleration of the platoon. Data collected during acceleration allows the calculation of the drag force on the trail-vehicle, while data collected during deceleration is used to calculate the drag on the lead vehicle. Results from the full-scale tests show that the drag behaviors for the two vans are in general agreement with the earlier conclusions drawn from the wind tunnel tests—namely, both vans experience substantial drag savings at spacings of a fraction of a car length.

I. INTRODUCTION

One of the new, state-of-the-art technologies to be employed within the Automated Highway System concept is the organization of freeway traffic into platoons of close-following vehicles. Close-following is achieved by utilizing computer control to automatically maintain a close spacing between the members of the platoon. As presently conceived, each vehicle is equipped with automatic throttle, brake and steering, as well as a means for determining accurate headway position and for communicating with other vehicles within the platoon. Earlier wind tunnel studies at USC have predicted that substantial drag savings can be achieved through close-following. For example, members of a 7-8 vehicle platoon are predicted to have an average drag approximately 1/2 the drag value experienced by each vehicle in isolation. Furthermore, all vehicles in the platoon participate in the drag savings. Lower values of drag translate directly to improvements in fuel economy and to a reduction in emissions.

II. OVERVIEW

Earlier wind tunnel studies at USC have predicted that substantial drag savings can be achieved through close-following. The studies utilized 1/8 scale model minivans at Reynolds numbers of approximately 10^6 based upon model length. Figure 1, reproduced from Zabat et al. (1995), shows measured drag coefficients for the simplest possible interaction—two close-following vehicles placed in tandem.

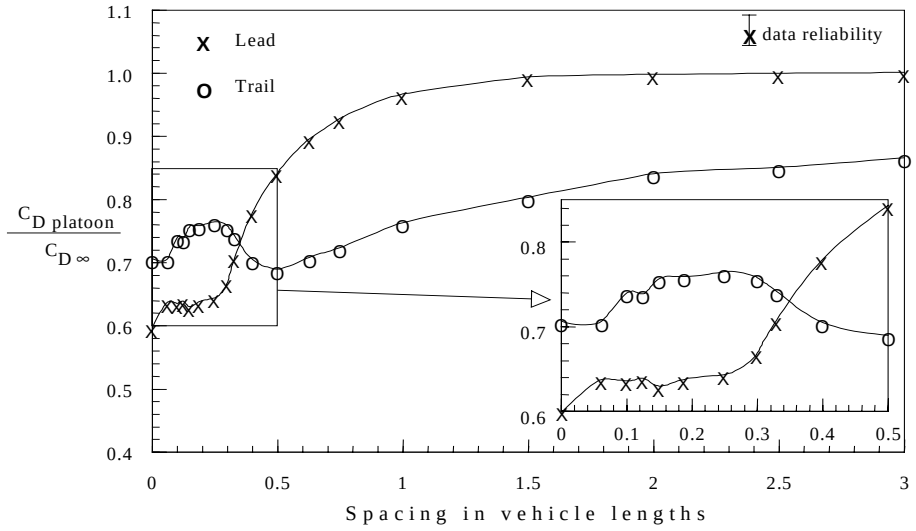

Figure 1. Drag coefficient predictions for two close-following vehicles.

The vehicle models are mounted on a porous ground plane, and a small suction is applied to remove unwanted boundary layer growth. The ordinate is the drag coefficient in close-following normalized by the drag of a single-vehicle in isolation. The drag results are surprising for they indicate a cross-over of the drag so that, at short spacings, the forward vehicle has a lower drag

coefficient than the trail vehicle. The particular separation for which the drag curves cross is a position of stable equilibrium in the following sense. If the separation between the two vehicles becomes shorter, the trail vehicle experiences more drag and will tend to drop back, and if the separation becomes greater, the trail vehicle experiences less drag and will gain. In each case the tendency is to return to the equilibrium position.

The result is counter to the general belief that the trail vehicle must always experience less drag because of favorable shielding by the lead vehicle. It also runs counter to the experience gained in a variety of racing situations, and most particularly from stock cars. We do not believe the results are inconsistent with the wisdom accumulated from the racing community. Our results place the point of drag reversal at about 0.3-0.4 vehicle lengths, or about 5-6 feet for a 16 foot vehicle. One would probably have to be closer than 4 feet to observe the effect of the reversal. After careful observation we have concluded that racing stock cars rarely run this close, although from an oblique camera view they sometimes appear to be closer. They are often observed to run at spacings of 1/3-1/2 vehicle length, which would be close to the projected equilibrium position.

The gross features of the drag dependence at close spacing do not depend upon the particular shape of the vehicle, but the details do depend upon geometry. Figure 2 shows the same two minivan models, but now operated in a reverse orientation, with the rear facing forward (also from Zabat et al. 1995).

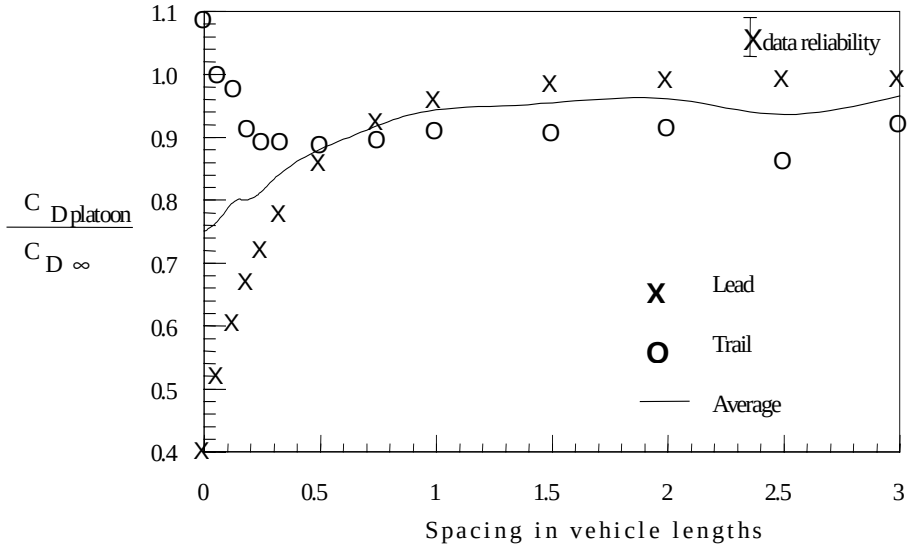

Figure 2. Drag predictions for two close-following vehicles in reverse orientation. Solid line is the average drag coefficient.

In this case, the drag cross-over spacing is greater, and there is no plateau appearing in the coefficient values at the shortest spacings. Figure 3 is the same two minivan models in proper

orientation, but now utilizing a non-porous ground plane (Zabat et al. 1995). Again there are differences in the details of the drag behavior, but the general features of the cross-over are preserved.

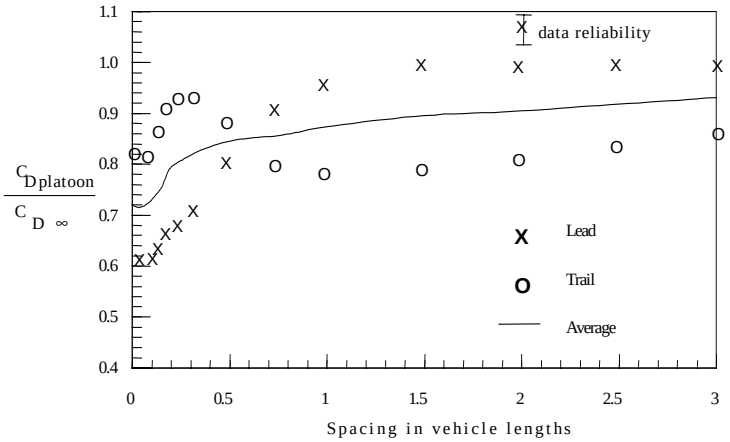

Figure 3. Drag predictions for two close-following vehicles, non porous ground plane. Solid line is the average drag coefficient.

PHYSICAL INTERPRETATION OF DRAG BEHAVIOR

The origin of the drag reversal can be understood in simplest terms by regarding the curvature of streamlines which enter and leave the gap region between the vehicles. Streamline curvature requires a pressure gradient from the center of the gap increasing towards the boundaries. This produces a positive pressure drag increment on the trail vehicle and a negative pressure drag

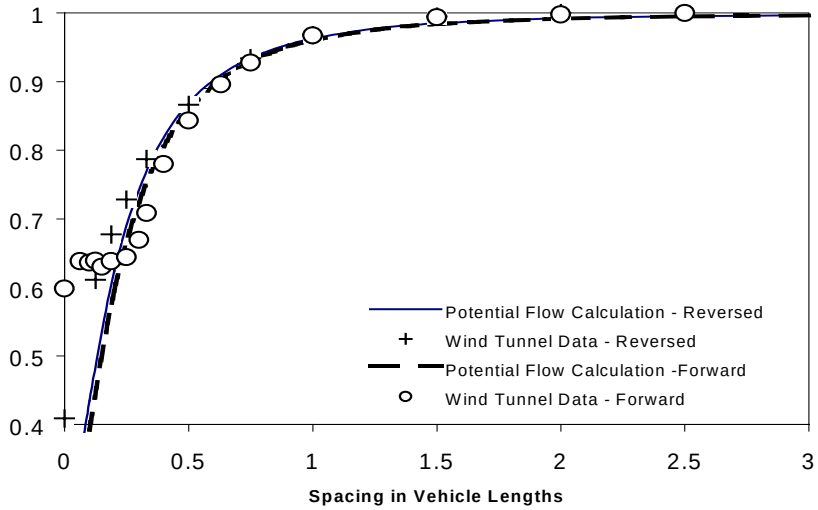

Figure 4. Prediction of incremental drag for lead vehicle of close-following pair

increment on the lead vehicle. The pressure drag increments become larger as the separation decreases because streamline curvature increases. This argument was tested by Browand, Zabat

& Tokumaru (1997) by performing an inviscid panel method calculation for two egg-shaped ellipsoids in tandem. The eggs are intended to approximate the geometry of the van models. The solid line and the dotted line in Figure 4 show the results of the calculation for the incremental drag on the forward egg due to the presence of the trailing egg corresponding to the orientations in Figures 1 and 2.

The results of this simple calculation agree remarkably well with the wind tunnel observations in spite of the obvious disparities in detailed geometry. (Of course the panel calculation will not capture the plateau at shortest spacings if, as we believe, it is produced by a strong separation/reattachment which effectively closes gap to significant inflow.)

Models in wind tunnels (and numerical computations) do not possess the complexity of real vehicles operating on a roadway at much higher Reynolds numbers. In the following sections, we describe the procedure developed to measure the drag of two full-scale vehicles operating at close spacing. The results are then compared with the wind tunnel observations.

III. FULL-SCALE DRAG MEASUREMENTS

THE TOW BAR

Two Ford Windstar vans are used for the field tests. One van is a gift from Ford Motor Company, and carries inverted power and instrumentation on board. The second van is a rental. The two Windstars are connected by means of a tow bar system sketched in Figure 5. A load cell in each arm of the tow bar measures the corresponding axial force between the two vehicles. The two-arm design provides lateral stability during testing at high speeds, a feature which cannot be achieved using a single-arm. The tow bar is also designed to be as aerodynamically unobtrusive as possible, and, in addition, meets the following criteria: connections to both the lead vehicle and trail vehicle are simple and non-destructive; a pulley system at the point of attachment to the lead vehicle facilitates the turning of the two vehicles during testing; different sets of tow cables provide vehicle spacings between 0.2 to 1.0 vehicle lengths; the tow bar remains horizontal during towing, and transmits moment-free horizontal forces to the load cells. There are no commercially available products to meet the above criteria; the tow bar and all attachment fixtures were designed and machined in-house at USC. The pulley mount for the lead vehicle attaches by means of available holes in the Windstar frame. The connection point for the cables is moved forward as far as possible to meet the minimum spacing requirement of 0.2 vehicle length.

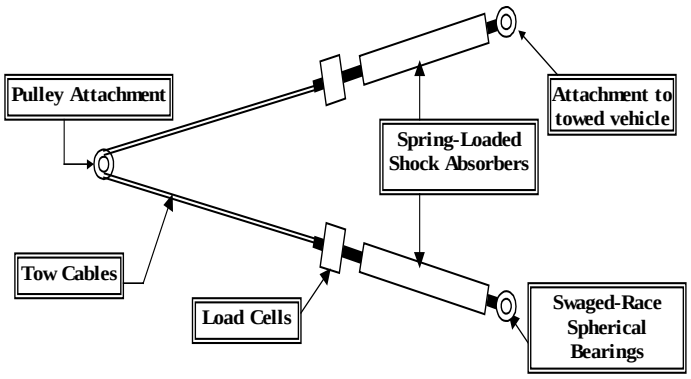

Figure 5. Schematic of the tow bar.

The trailing car attachments are also easily installed on the chassis of the Windstar. A trailing support tube runs the width of the van, in front of the bumper, and is supported by brackets that are connected to the chassis just below the front bumper. The tube supports a mounting fixture to receive the spherical bearings at the trailing ends of the tow bar.

TOW BAR DYNAMICS MODEL

Linear springs and dampers are placed in each leg of the tow bar to remove as much road noise as possible from the load-cell signal. A longitudinal stability model is developed to study the dynamics of the two vehicles and the tow bar. The results of the analysis are used to size the springs and shocks to provide a predetermined level of low pass filtering. (A detailed discussion of the tow bar and the dynamics model can be found in the report by Hong et al. 1997.) Based on the tow bar dynamics model, a spring rate of 120 lbf/in (60 lbf/in in each unit), with the damping rate at approximately 200 lbf/ft/sec (100 lbf/ft/sec in each unit) is chosen. The damping rate is achieved by using silicone oil with the appropriate viscosity. Oil is stored in a simple sleeve-type accumulator surrounding the spring-loaded shocks (from Works Performance Shocks, Northridge, California). With these values, the design cut-off frequency is approximately 0.78 Hz, and the equilibrium spring extension is between 1-2 inches for vehicle spacing in the range of 0.2 - 1.0 vehicle length. The steady state force in each arm of the tow bar is estimated to be less than 90 lbf with vehicles traveling between 40 mph and 70 mph. Each load cell has a maximum capacity of 250 lbf (Sensotec, Inc), and provides additional margin for forces experienced by the acceleration of the two vehicles. The load cells are calibrated by mounting the entire tow bar in a vertical position on a specially designed steel-framed cart. Weights are applied by means of the same cable and pulley arrangement used to connect the two vehicles.

OPTICAL SENSOR

The Datron optical speed sensor (on loan from *Road & Track Magazine*) provides an analog estimate of forward speed by performing a real time cross-correlation of the signals from a pair of sensors. These two sensors receive reflected illumination from two small patches of the

roadbed displaced in the direction of travel. The cross correlation of the two signals peaks at a time interval which is linearly dependent upon forward speed. The sensitivity of the Datron is approximately 40 mV per mile per hour (25 mV per kilometer per hour).

DATA ACQUISITION

Data recording is by means of a Pentium-75 laptop computer utilizing a National Instruments DAQ-700 A/D PCMCIA card. Data from the Datron and from the load cells are downloaded into the computer via the DAQ-700 card using a customized LabView data acquisition program. LabView is an extremely flexible programming language based upon function blocks or VI's (virtual instruments). For example, a VI dedicated to reading data from the DAQ-700 board can be called from either the calibration program or the field test program. Different programs can be constructed from these basic VI blocks to meet the needs of the application. The 12-bit (4096 levels) A/D interface board is set to read +/- 5 volts full-scale output. For the Datron, the least bit accuracy is +/- 0.06 mph. For the load cell, the least bit accuracy is approximately +/- 0.12 lbf. A flow chart of the data acquisition system is shown in Figure 6. The scan rate is set to approximately 160 digitizations per second. A typical run may last 200 seconds, and there may be 50 runs per day for a total record of perhaps 6-10 megabytes.

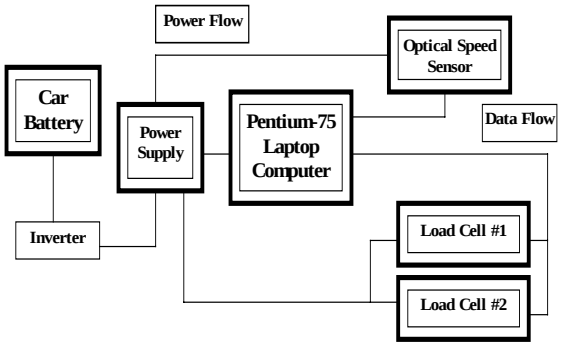

Figure 6. Data acquisition flow chart.

FIELD SITE REQUIREMENTS

The two-vehicle drag measurements require a site having near-zero wind speed, a near-flat, smooth surface, and enough space for acceleration and deceleration of the vehicles. After researching several possible locations in Southern California, El Mirage dry lakebed near Victorville, California, was selected. At El Mirage, after all the moisture from winter has evaporated, the surface is flat and very smooth. The expansive area of the dry lakebed also allows for safe vehicle operations, especially necessary when the vehicles are traveling at high speeds at close spacing. A complete experimental run requires a straight line distance of approximately 2.5 miles for acceleration and deceleration. Experimental runs usually commence at daybreak and conclude at the earliest sign of steady wind—usually about 10:00 AM.

PROTOCOL FOR TESTING

The vehicles begin a typical run from a standing start and accelerate slowly to a speed of 75-85 mph. Figure 7 shows the tow bar installed between the two vehicles at the commencement of a test. During the acceleration phase, the trail vehicle remains in neutral with the lead vehicle pulling. We refer to the acceleration portion as the pull-up phase. In many of the tests the trail vehicle is equipped with free-wheeling hubs on the drive wheels.

Figure 7. Vehicles at commencement of a typical test run.

Free-wheeling hubs completely remove the transmission (and engine) from drag consideration. When a sufficiently high speed is attained—and this speed will vary slightly from run to run, and for different spacings—the lead vehicle is then placed in neutral, commencing the coast-down phase. During coast-down, the trail vehicle applies slight braking to insure that tension is maintained in the tow bar. A single run consists of pull-up and coast-down. Six to eight similar runs are repeated—half in each direction—along the axis of the lakebed. A typical run is photographed in Figure 8, and illustrates the major disadvantage of testing at El Mirage. A thin layer of fine clay particles is present on the surface of the lakebed. When operating in close-following, this layer is swept up by the lead vehicle and accumulates in the region between the vehicles and in the downstream wake. It is impossible to keep dust away from the interior of the trail vehicle, and the driver and the computer operator in that vehicle must use face masks similar to those used when spraying paint. The dust does allow the wake flow to be visualized. Figure 8 shows an interesting periodic wake structure, which we believe to be caused by the alternate shedding of vorticity from the sides and the roof of the trail vehicle.

Figure 8. Two vehicles close-following at El Mirage dry lakebed.

IV. DATA ANALYSIS AND RESULTS

SINGLE VEHICLE COAST-DOWN

Coast-down data consists of a record of vehicle velocity versus time, recorded at a rate of 160 digitizations per second. The analysis is based upon the dynamic equation of motion for the vehicle decelerating on a horizontal surface:

$$M\frac{dV}{dt} = -F_D - F_R \tag{1}$$

Here, M is the mass of the vehicle, V is the speed of the vehicle, and F_D, F_R are the aerodynamic drag and rolling resistance forces, respectively. El Mirage lakebed is as flat and horizontal as can be achieved in practice. Over time, more than 100 runs were made in both directions along the axis of the lakebed, and no consistent difference attributable to a slight gradient in slope was observed.

The drag and the rolling resistance forces oppose the motion of the vehicle during a coast-down. The resistance force, F_R, has been found by several authors [Passmore and Le Good 1994, Buckley 1978, Yasin 1978] to vary approximately linearly with the vehicle speed.

$$F_R = a_0 + a_1 V \tag{2}$$

The drag force, F_D, is, of course, quadratic in the relative wind speed (the vector addition of vehicle speed and ambient wind). All of the tests were conducted under conditions of no-wind. Air over the lakebed is quite stable in the early morning, and no-wind conditions are common. The majority of the tests were performed between dawn and about 10:00 AM. If at any time the wind increased above two meters per second (about 4 mph), testing would be suspended. Usually the wind speed was considerably less that 4 mph, so that to a sufficient degree of approximation, the drag becomes quadratic in vehicle speed.

$$F_D = b_2 V^2 \tag{3}$$

The coefficient b_2 is shorthand for the $b_2 = \frac{1}{2}\rho A C_D$ quantity where A is the frontal area of the vehicle, ρ is the air density and C_D is the non-dimensional drag coefficient.

It is because of the different dependencies upon speed that the drag coefficient of the vehicle can be extracted from coast-down data. However, there are other quadratic velocity dependencies in addition to drag which will introduce uncertainties in the value of the drag coefficient. Fortunately, most of the additional quadratic contributions are small. We will present results for the drag coefficient in close-following as a fraction of the drag coefficient in isolation. When both terms of the ratio contain the identical small parasitic contributions, the effect upon the ratio is even smaller. The largest of these parasitic quadratic contributions arises from complicated fluid motions within the transmission, and will be considered explicitly. We have conducted two

separate experiments. In one experiment, coast-down proceeds with the vehicle transmission set in "Neutral" position. In the second experiment, termed "Hubs", the transmission is removed from consideration by installing free-wheeling hubs on the drive wheels. By comparing the values of the coefficient b_2 between the two sets of coast-down experiments, the effect of the transmission will be isolated for future application.

With these assumptions, one can model the two forces in equation (1) in terms of speed, V, and equation (1) becomes:

$$M\frac{dV}{dt} = -a_0 - a_1 V - b_2 V^2 \tag{4}$$

Two methods are used to extract the coefficients. The first method is to numerically differentiate the $V = V(t)$ signal, and then to fit a quadratic polynomial in V to the right hand side in a least square sense. The three coefficients a_0, a_1 and b_2, are therefore determined directly. This method is noisy, since the velocity signal must be differentiated. It is used primarily as a check for the second method, which is based upon an integration of equation (4).

The time integration method has been used in literature [Passmore and Le Good, 1994] with good reliability. We present a slight variation of this method. Time integration of equation (4) from a time t_0 to a later time t_n yields:

$$M(V(t_n) - V(t_0)) = -a_0(t_n - t_0) - a_1\int_{t_0}^{t_n} V dt - b_2\int_{t_0}^{t_n} V^2 dt \tag{5}$$

Since the data to be processed is discrete, the integrals in the equation above are replaced with summations. By varying the point in time $t_n = t_0 + n\Delta t$ to successively increasing time intervals $n = 1..N$, and applying (5) at each time step, one obtains a set of N equations and 3 unknowns, where $N+1$ is the number of data points, and the unknowns are a_0, a_1 and b_2. By setting the arbitrary time $t_0 = 0$, the set of N equations can be written as:

$$\boldsymbol{T}_n = a_0\boldsymbol{t}_n + a_1\boldsymbol{X}_n + b_2\boldsymbol{Y}_n \tag{6}$$

Where:

$$\boldsymbol{T}_n = M(V(t_0) - V(t_n))$$

$$\boldsymbol{X}_n = \sum_{k=1}^{n}(V(t_k) - \frac{V(t_0)}{2} - \frac{V(t_n)}{2})\Delta t$$

$$\boldsymbol{Y}_n = \sum_{k=1}^{n}(V^2(t_k) - \frac{V^2(t_0)}{2} - \frac{V^2(t_n)}{2})\Delta t$$

The system of equations (6) is solved for a_0, a_1 and b_2. by fitting a linear polynomial

$$T = a_0 t + a_1 X + b_2 Y$$

to the data points selected, in the least square sense.

The b_2 coefficients are translated to values of $C_D A$ by using local temperature and pressure data to determine the appropriate air densities. Temperatures are recorded locally throughout the test periods, and hourly barometric pressure is obtained from nearby Edwards Air Force Base (elevation 2292 feet) and extrapolated to the elevation of the El Mirage lakebed (elevation 2865 feet).

Transmission set to "Neutral" position

Coast-down begins from a speed of approximately 80-85 mph, after the vehicle has been placed in neutral and a steady deceleration has been established. Since the raw velocity record contains information prior to the establishment of a steady deceleration, the data record is trimmed at the higher speed end to a value referred to as the trim limit speed, V_{TL}. The greatest usable speed range varies from run to run, and is not known precisely. Consequently, calculations are made for successively higher values of the trim limit speed; the data record from each coast-down run is divided in several subsets by taking speed intervals from the low cut-off value of 20 mph up to 50 mph, then from the low cut-off value up to 51 mph and so on, up to the maximum speed in the data record. The results are then plotted versus the increasing values of the trim limit speed V_{TL} . These plots are shown in Figures 9a, b and c. (Since the maximum speed of each set is not exactly the same, the right ends of the curves occur at different values of V_{TL}). The results from ten separate coast-downs are shown in dotted lines. The average curves (continuous thick lines) shown in Figure 9a, b, and c are the average for all ten separate runs over a range of trim limit speed from 50 mph to the *min(max(Vi))*, where $i = 1..10$. A slight additional smoothing is achieved--the heavy dotted curve--by fitting the average curve to a second-order polynomial in V_{TL}.

Coast-down with "Free-wheeling" hubs

Data is also processed from thirteen separate coast-down runs with free-wheeling hubs mounted on the front wheels. As before, calculations at successively increasing values of trim limit speed are made for each run, and the results are shown in Figures 10a, b, and c. In all these runs, the tow cable was released at approximately 78 mph, and a steady deceleration was established at approximately 72 mph. This must be regarded as the upper limit of reliable data. Again, the thick continuous line is the average, and the dotted line is a fit of the average curve with a quadratic polynomial in V_{TL}.

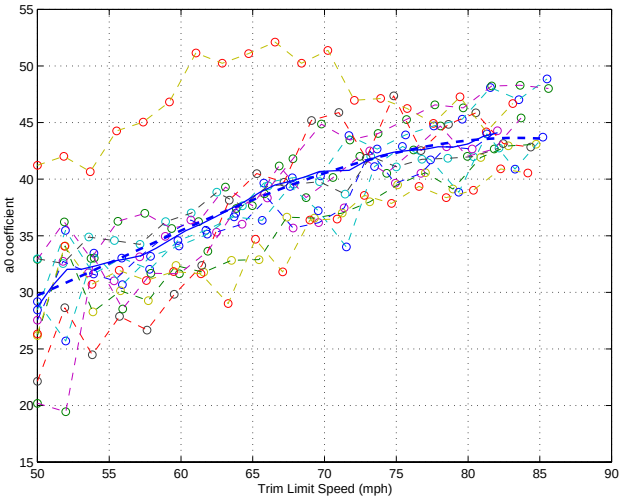

Figure 9a. Variation of the coefficient C_DA with increasing values of trim limit velocity V_{TL}, for the coast down tests with the transmission set to "Neutral" position.

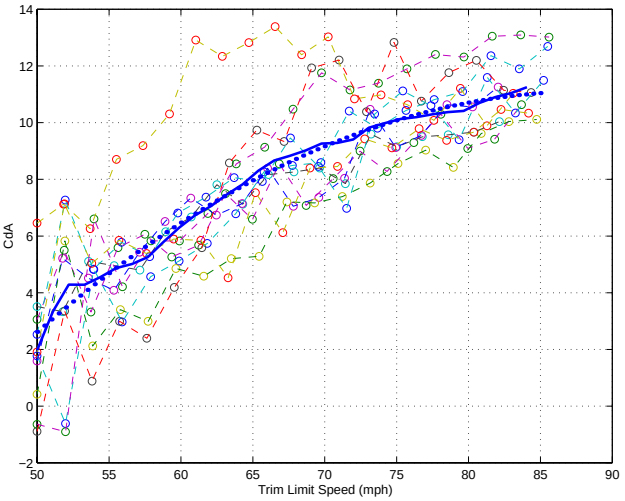

Figure 9b. Variation of the coefficient a_1 with increasing values of trim limit velocity V_{TL}, for the coast down tests with the transmission set to "Neutral" position.

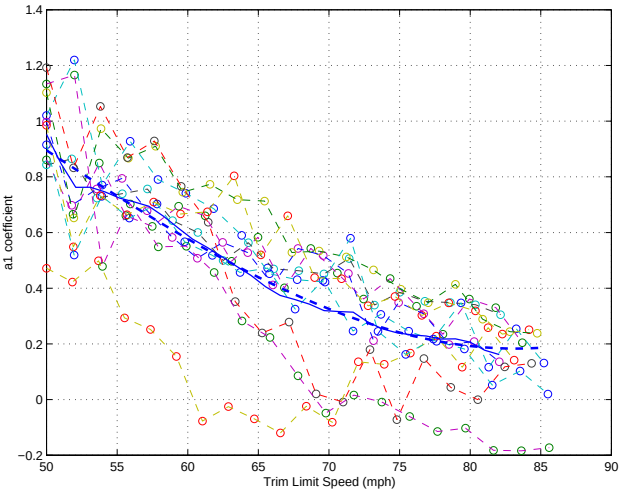

Figure 9c. Variation of the coefficient a_0 with increasing values of trim limit velocity V_{TL}, for the coast down tests with the transmission set to "Neutral" position.

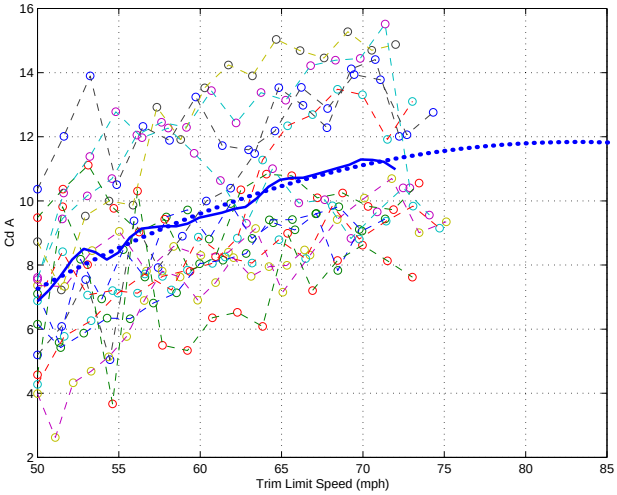

Figure 10a. Variation of the coefficient C_DA with increasing values of trim limit velocity V_{TL}, for the coast down tests with free-wheeling hubs.

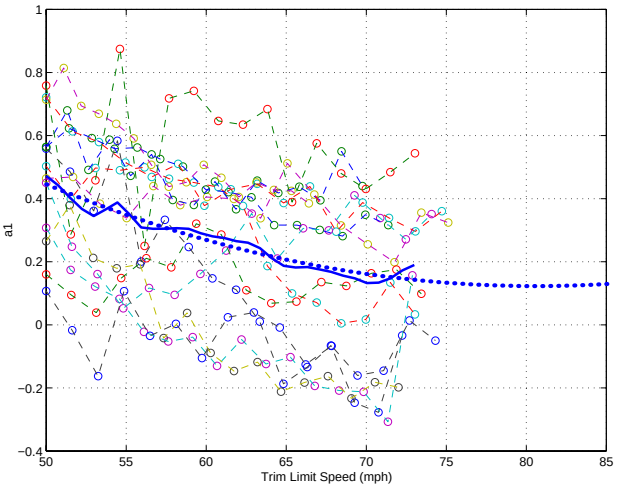

Figure 10b. Variation of the coefficient a_1 with increasing values of trim limit velocity V_{TL}, for the coast down tests with free-wheeling hubs.

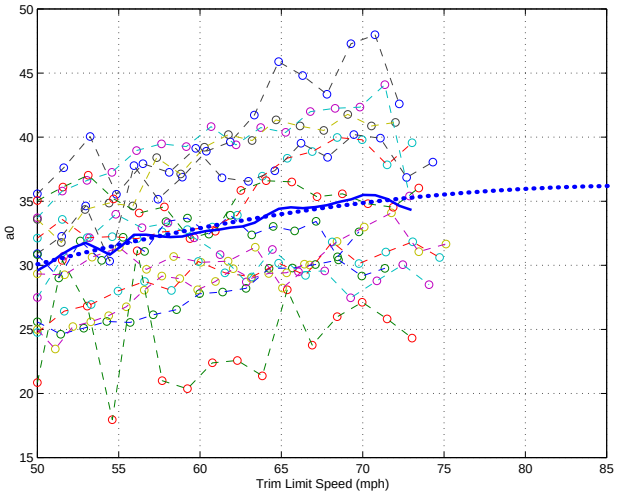

Figure 10c. Variation of the coefficient a_0 with increasing values of trim limit velocity V_{TL}, for the coast down tests with free-wheeling hubs.

DRAG DETERMINATION FOR AN ISOLATED VEHICLE

The first conclusion from the results of Figures 9 and 10 is that all the coefficients depend upon the value of the trim limit speed. The value of a_0 is relatively stable but increases by about twenty five percent as trim speed increases from 50 to 70 mph. Both a_1 and C_DA are more sensitive to changes in trim speed. The implication is that a sufficient range of speed must be available to properly fix the coefficient values, but one might have expected the values of a_0, a_1, and C_DA to become independent of trim speed once an adequate speed range is established. All three coefficients do change less rapidly as the trim speed increases, and all three appear to be reaching an asymptote. This is particularly evident in Figure 9, where the speed range extends to the higher values of approximately 85 mph. In fact, all the quadratic polynomial fits (heavy dotted lines) approach zero slope in the 80-85 mph range.

The amount by which the three coefficients a_0, a_1, and C_DA vary with V_{TL} has been analyzed using a $V=V(t)$ signal generated by numerically integrating (4) for known values of the a_0, a_1, and b_2 coefficients. The computer generated $V(t)$ signal was processed the same way as the measured signal, first clean, and then with 1-3% of white noise added. The results showed a significantly larger variation of the a_0, a_1, and C_DA with V_{TL} when noise is added. Therefore the noise in the measured signal is responsible for the dependency of the a_0, a_1, and C_DA coefficients with the trim limit speed values. Nonuniformities of the lakebed surface also add small random perturbations to the signal, thus increasing the dependency effect.

In the case of free-wheeling hubs, the necessity for disconnecting and aerodynamically separating from the tow vehicle, effectively limits the usable trim speed to 70-72 mph. In the range 50-70 mph, there is less variation in all three coefficients, and this fact suggests that the powertrain is responsible for a considerable portion of the variation. In making an honest comparison between the two cases, one must choose the identical trim limit speed. There are two reasonable choices. One is to use the greatest reliable speed for the free-wheeling hubs, the value of 70 mph, and then evaluate the coefficients at this same speed for the "neutral" case. The second choice is to use the best values for the "neutral" case in the 80-85 mph range, and extrapolate the "free-wheeling" hubs result to this speed using the polynomial fit (heavy dotted line in 10). We choose the second method. For comparison purposes, the values of the three coefficients for each case are shown in the table below:

	"Free-wheeling"	"Neutral"	
a_0	36.19	43.50	(Units are lbf)
a_1	0.13	0.19	(when V is in feet/sec)
C_DA	11.83	11.04	(when V is in feet/sec)

All three of the estimated coefficients differ between the two cases. The value a_0 measures the rolling resistance, and is sometimes written Mgr_0, where r_0 is the coefficient of the rolling resistance. The value a_1 is a rolling resistance correction to account for slight velocity dependence $a_1=Mgdr_0/dV$. These values may indeed differ in the two experiments, because the runs are made at different times over slightly different test paths on the lake-bed. However, the values of C_DA also differ, and somewhat surprisingly. The estimate for the value of C_DA is

greater when the transmission is disconnected by use of free-wheeling hubs. Evidently, the engagement of the transmission contributes a small quadratic dependency on speed, containing a negative coefficient. Although we do no understand the details of the transmission effects, discussions with Ford engineers have verified the possibility of a negative coefficient. Our best estimate for the drag coefficient, C_DA, of the Windstar van would be the value with the free-wheeling hubs. It is about ten percent higher than values reported for the Windstar by Ford Motor Company. We regard this as a reasonable agreement.

TWO CLOSE-FOLLOWING VEHICLES

Each run consists of an acceleration phase, the pull-up, in which the driving/accelerating force is provided by the lead vehicle of the two vehicle platoon, followed by a deceleration, the coast-down phase, during which slight breaking is provided by the trail vehicle to insure that a tension is continuously maintained in the tow bar. The acceleration portion provides data for the calculation of drag on the trail vehicle, and the deceleration portion provides data for calculation of drag on the lead vehicle.

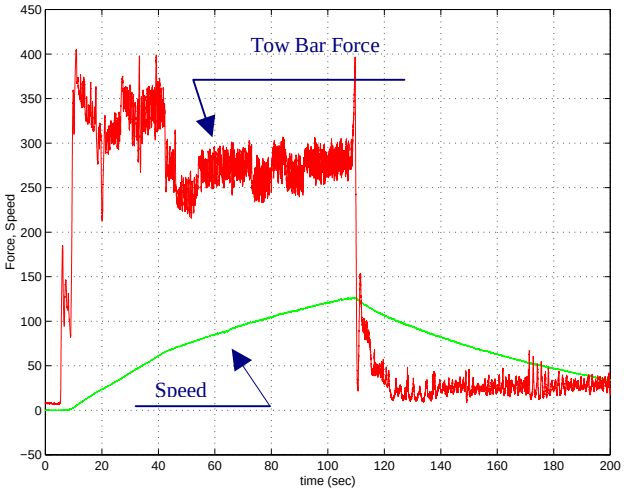

Figure 11. Typical example of a data set obtained from a tow test run.

Each continuous data record must be divided into subsets corresponding to the acceleration and deceleration portions of the test, which are to be processed separately. Data obtained from the two close-following vehicles are digitized records of vehicle speed and tow bar force versus time, acquired at a rate of 160 digitizations per second.

A typical example of a data set obtained from a combined pull-up coast-down run is shown in Figure 11. The vertical axis reads tow-bar force (lbf), or vehicle speed (ft/sec).

Numerically, it is straightforward to separate the data set into separate acceleration and deceleration subsets. The moment in time when maximum speed is reached is computed first. Then, the acceleration subset is selected from the beginning of the record up to the point of maximum speed, while the deceleration subset is selected from the point of maximum speed to the end of the record. However, there are additional considerations. Time must be allowed for the drivers to coordinate a shift into neutral, and for slight braking to commence. Thus an eight second time interval, centered at the point of maximum speed, is ignored in the data record.

For each data subset, processing is based on the dynamic equation of motion. The only difference now is the addition of the tow bar force. Taking into consideration, as previously discussed, the dependencies of rolling resistance and aerodynamic drag upon vehicle speed, the equation of motion becomes:

$$M\frac{dV}{dt} = F_{TB} - (a_0 + a_1 V) - b_2 V^2 \tag{7}$$

The sign in front of the tow-bar force, F_{TB}, is positive for the pull-up of the trail vehicle, and negative for coast-down of the lead vehicle, and again, the b_2 coefficient represents aerodynamic drag, $b_2 = {}^1/_2 \rho\, C_D A$.

The time integration method is used to process both acceleration and deceleration phases. Each data subset is integrated with respect to time from an initial point in time t_{0a}, or t_{0b} (for the acceleration and deceleration subsets respectively) to a final point in time , time t_{na}, or t_{nb}. For example, the pull-up phase is represented by

$$M(V(t_{na}) - V(t_{0a})) = \int_{t_{0a}}^{t_{na}} F_{TB}\,dt - a_0(t_{na} - t_{0a}) - a_1 \int_{t_{0a}}^{t_{na}} V\,dt - b_2 \int_{t_{0a}}^{t_{na}} V^2\,dt \tag{8}$$

In a similar manner to the description presented for the coast-down of a single vehicle, the integrals in the equations above are replaced by summations over successively increasing time intervals, obtaining for each data subset a system of N equations with 3 unknowns. Additionally, one can consider $t_{0a} = 0$ and $t_{0n} = 0$ since these are arbitrary initial moments. With these considerations, the system of N equations with the 3 unknowns a_0, a_1 and b_2 can be written as follows:

$$\pm \boldsymbol{T}_n = a_0 t_n + a_1 \boldsymbol{X}_n + b_2 \boldsymbol{Y}_n \tag{9}$$

$$\boldsymbol{T}_n = M(V(t_0) - V(t_n)) + \boldsymbol{F}_n$$

$$\boldsymbol{F}_n = \sum_{K=1}^{n} F_{TB}(t_k) - \frac{F_{TB}(t_1)}{2} - \frac{F_{TB}(t_n)}{2}$$

$$\boldsymbol{X}_n = \sum_{k=1}^{n} (V(t_k) - \frac{V(t_0)}{2} - \frac{V(t_n)}{2})\Delta t$$

$$\boldsymbol{Y}_n = \sum_{k=1}^{n} (V^2(t_k) - \frac{V^2(t_0)}{2} - \frac{V^2(t_n)}{2})\Delta t$$

where the (+) sign corresponds to the acceleration part while the (-) sign corresponds to the deceleration part. The various terms represent:

The system of equations is solved for a_0, a_1 and b_2 by fitting a linear polynomial

$$T = a_0 t + a_1 X + b_2 Y$$

to the data points selected, in the least square sense. As before, calculations are made for the three coefficients for successively increasing values of trim limit speed. Data is obtained from two, separate experiments; the first, S1 conducted on October 17-18, 1996, and the second, S2, conducted on July 15-17, 1997. For S1, platoon experiments consisted of eight identical runs for each of the three vehicle spacings. During the second session, S2, platoon experiments consisted of eight runs for each of the six spacings. All together data from 72 separate runs is processed.

DRAG DETERMINATIONS FOR TWO VEHICLES

Following the procedures described for the single vehicle coast-downs, the C_DA values are determined for trail and lead vehicle as averages of all the runs at each separation. For the trail vehicle, the ratios of drag coefficient to drag coefficient in isolation are presented in Table 3.1.a and 3.1.b for sessions S1 and S2 respectively.

Car Spacing (car lengths)	$\frac{C_D}{(C_D)_{Neutral}}$
0.35	0.7300
0.53	0.6441
0.98	0.7529

Table 3.1.a. Quadratic coefficients, acceleration phase, session S1, trail car.

Car Spacing (car lengths)	$\frac{C_D}{(C_D)_{Hubs}}$
0.2344	0.7278
0.2865	0.6657
0.3802	0.6978
0.5521	0.6259
0.7448	0.6724
1.0000	0.7379

Table 3.1.b. Quadratic coefficients, acceleration phase, session S2, trail car.

(In session S1, the trail car was run with transmission set to "Neutral" position, while in the S2 session the trail car had free-wheeling hubs mounted on the driving wheels).

Similar results for the lead vehicle are presented in Tables 3.2.a and 3.2.b, for sessions S1 and S2 respectively. Note however that the lead vehicle must always operate with transmission in "neutral".

Car Spacing (car lengths)	$\frac{C_D}{(C_D)_{Neutral}}$
0.35	0.7124
0.53	0.7000
0.98	0.8877

Table 3.2.a. Quadratic coefficients, deceleration phase, session S1, lead car.

Car Spacing (car lengths)	$\frac{C_D}{(C_D)_{Neutral}}$
0.2344	0.6380
0.2865	0.5910
0.3802	0.6111
0.5521	0.7848
0.7448	0.8808
1.0000	0.9541

Table 3.1.b. Quadratic coefficients, deceleration phase, session S2, lead car.

The results from Tables 3.1 and 3.2 are plotted in the Figure 12 along with the wind tunnel results for the two-vehicle platoon (from Figure 1). An interpolating cubic spline has been drawn through the wind tunnel data.

Our estimates of the accuracy of the field test results are indicated by the error bars, and a least squares cubic spline fit is passed through this data. It is immediately clear that the full scale test results parallel the wind tunnel results in most important respects. At short spacing the drag of the trail vehicle exceeds the drag of the lead vehicle, as predicted from the wind tunnel tests. The major difference is that the full scale tests predict even lower drag coefficients by about ten per cent for both vehicles at almost all spacings. Also the equilibrium point defined by the crossing of the drag curves is displaced from the wind tunnel value of about 0.38 to a value of about 0.43.

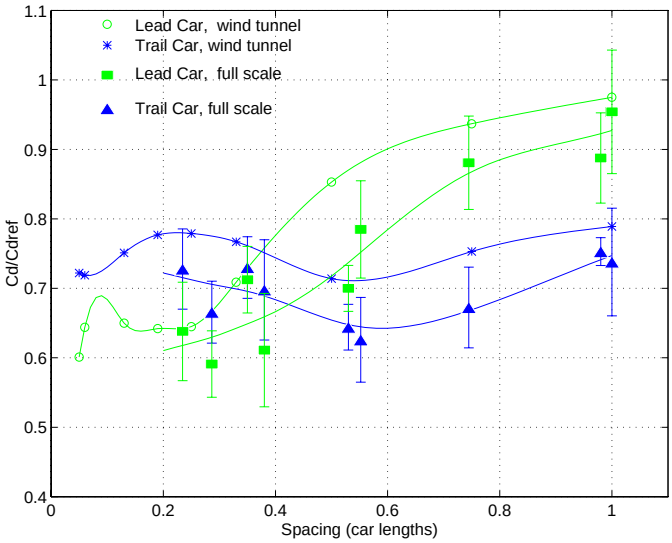

Figure 12. Aerodynamic drag coefficient ratios for a full-scale two-car platoon: a comparison to the wind tunnel 1/8 scale results.

V. FINAL SUMMARY

The drag reduction for a two-vehicle platoon is documented by an extensive set of full scale experiments conducted on El Mirage dry lakebed, using two Ford Windstar minivans. The drag forces are measured with the aid of a tow bar designed and manufactured at USC. Three series of experiments were carried out: i) coast-down experiments for a single vehicle with transmission set to "Neutral" position; ii) coast-down experiments for a single vehicle with "Free-wheeling" hubs mounted on the drive wheels (to eliminate transmission/engine influences); iii) two-vehicle close-following experiments consisting of an acceleration phase and a deceleration phase. The acceleration phase allows estimation of the drag of the trail vehicle, and the deceleration phase provides an estimate for the drag of the lead vehicle. Two separate sets of tow bar data are analyzed. Processing the recorded data utilizing a time integration method was chosen, following previous reliable results from several different authors.

Estimation of the drag of both vehicles in the platoon as a fraction of the drag of a vehicle in isolation is obtained for spacing between 0.23 vehicle lengths to 1.0 vehicle lengths. The drag ratio curves display a dependency on vehicle spacing similar to the wind tunnel results obtained using 1/8 scale models. Namely, at close spacings, the lead vehicle experiences less drag than the trailing vehicle. The reversal occurs at a spacing of about 0.43 vehicle lengths, compared to the wind tunnel prediction of 0.38 lengths. The drag reductions observed for the full scale vehicles are 5-10% greater than the results obtained in the wind tunnel.

ACKNOWLEDGMENT

Support for this research program was provided by the California Department of Transportation, under a grant administered through PATH Program, Berkeley, California.

Important contributions to the experiments have been made by Dr. Mustapha Hammache and the USC undergraduate students Paul Runyan and Christian Sharpe. Logistic support and technical assistance have been provided by the USC technicians Thane Dewitt and Mark Trojanowsky. At the El Mirage Lake location, California, constant help with weather conditions has been kindly provided by George Calloway.

REFERENCES

[1] Browand, F., Zabat, M. & Tokumaru, P.; 1997; “Aerodynamic Benefits from Close Following. *Automated Highway Systems*", ed. P Ioannou, Plenum Press, Chapter 12.

[2] Buckley, F. T. et al.; 1976; "Analysis of a Coast Down Data to Assess Aerodynamic Drag Reduction on Full Scale Tractor Trailer Trucks in Windy Environments", *SAE Paper No. 760850*.

[3] Hong, P., Browand, F. & Marcu, B.; 1997; "Design, Fabrication and Calibration of a Vehicle Tow Bar for Platoon Drag Measurements: A Working Report", *California PATH Working Paper UCB-ITS-PWP-97-2*.

[4] Janosi, P. Z.; 1996; "Windstar Coast Down Results", private communication.

[5] Passmore, M. A. & Le Good, G. M.; 1994; "A Detailed Drag Study Using the Coast Down Method", *SAE Paper No. 940420*.

[6] Yasin, T. P.; 1978; "The Analytical Basis of Automobile Coast Down Testing*", SAE Paper 780338.*

[7] Zabat, M., Stabile, N., Frascaroli, S. & Browand, F.; 1995; "Drag Forces Experienced by 2, 3 & 4-Vehicle Platoons at Close Spacings", *SAE Paper No. 940421*.